Dispersion anomalies in cuprate superconductors

A. V. Chubukov
Department of Physics, University of Wisconsin, Madison, Wisconsin 53706, USA

M. R. Norman
Materials Science Division, Argonne National Laboratory, Argonne, Illinois 60439, USA

(Received 7 February 2004; published 11 November 2004)

We argue that the shape of the dispersion along the nodal and antinodal directions in the cuprates can be understood as a consequence of the interaction of the electrons with collective spin excitations. In the normal state, the dispersion displays a crossover at an energy where the decay into spin fluctuations becomes relevant. In the superconducting state, the antinodal dispersion is strongly affected by the (π,π) spin resonance and displays an *S* shape whose magnitude scales with the resonance intensity. For nodal fermions, relevant spin excitations do not have resonance behavior, rather they are better characterized as a gapped continuum. As a consequence, the *S* shape becomes a kink, and superconductivity does not affect the dispersion as strongly. Finally, we note that optical phonons typically lead to a temperature-independent *S* shape, in disagreement with the observed dispersion.

DOI: 10.1103/PhysRevB.70.174505 PACS number(s): 74.25.Jb, 74.72.Hs, 79.60.Bm, 74.50.+r

I. INTRODUCTION

Angle resolved photoemission (ARPES) experiments are valuable sources of information about the shape of the Fermi surface in the cuprates and the frequency, momentum, and temperature dependence of the electron self-energy. The subject of this paper is an analysis of the dispersion along various momentum cuts. These dispersions have been obtained by several groups[1–10] via high-precision measurements of the momentum distribution curves (MDCs), by which the spectral function is obtained at a given energy by making scans along directions normal to the Fermi surface. The spectral function $A(\mathbf{k},\omega)=(1/\pi)|\mathrm{Im}\,G(\mathbf{k},\omega)|$ is related to the self-energy $\Sigma_{\mathbf{k}}(\omega)$ as

$$A(\mathbf{k},\omega)=\frac{1}{\pi}\frac{\Sigma''_{\mathbf{k}}(\omega)}{[\omega-\epsilon_{\mathbf{k}}-\Sigma'_{\mathbf{k}}(\omega)]^2+[\Sigma''_{\mathbf{k}}(\omega)]^2}. \quad (1)$$

Near the Fermi surface, $\epsilon_{\mathbf{k}}\approx v_F(\mathbf{k}_F)(k_\perp-k_F)$, where $v_F(\mathbf{k}_F)$ is the bare value of the velocity. There are several reasons (both theoretical and experimental) to believe that the self-energy weakly depends on the value of $k_\perp$ normal to the Fermi surface, and can be approximated as $\Sigma_{\mathbf{k}}(\omega)\approx\Sigma_{\mathbf{k}_F}(\omega)$. For a given $\mathbf{k}_F$ specified by a cut, the MDC spectral function $A(k_\perp,\omega=\mathrm{const})$ is then a Lorentzian centered at $v_F(\mathbf{k}_F)(k_\perp-k_F)=\omega-\Sigma_{\mathbf{k}_F}(\omega)$ with a half width at half maximum (HWHM) equal to $\Sigma''_{\mathbf{k}_F}(\omega)/v_F(\mathbf{k}_F)$ (Ref. 3). In a generic Fermi liquid, the self-energy is linear in ω at the lowest energies: $\Sigma'_{\mathbf{k}_F}(\omega)=-\lambda_{\mathbf{k}_F}\omega$. The position of the MDC peak then determines the renormalized Fermi velocity $v_F^*=v_F/(1+\lambda_{\mathbf{k}_F})$. At higher energies, λ becomes frequency dependent, and the dispersion deviates from the linear form.

The MDC data have revealed several characteristic features of the dispersion that need to be explained:

(a) In the normal state, the dispersion along both the nodal and antinodal directions shows a relatively smooth crossover from a linear behavior at small binding energies to a more steep behavior above roughly 50-70 meV. This effect has been observed in Bi2212,[1–5,8] Bi2201,[4,8] Bi2223,[8] Na_xCCOC,[6] and LSCO.[4,7] In the last case, the crossover is sharper and more resembles a kink.

(b) The renormalized Fermi velocity v_F^* along the nodal direction weakly depends on doping[7] and in Bi2212 equals 1.6 eV Å.[3,7] At the same time, at high energies, the dispersion is strongly doping dependent, becoming steeper with underdoping.[5,7]

(c) In the superconducting state, the dispersion along the antinodal direction develops an *S* shape,[11] with a "negative" dispersion between 60 and 80 meV. This feature develops with decreasing temperature in an order-parameter-like fashion, with an onset temperature at T_c for overdoped samples, and somewhat above T_c for underdoped samples.[8,10]

(d) The dispersion along the nodal direction does not develop an *S* shape below T_c. Instead, in the superconducting state the crossover gets sharper, with a kinklike feature near 70 meV developing in Bi2212 (Refs. 2–5 and 8) and Bi2223 (Ref. 8). This extra "sharpness" has a temperature dependence similar to that of the antinodal dispersion mentioned above.[5] In Bi2201 and LSCO, on the other hand, the nodal dispersion does not change much between the normal and superconducting states.[4,8]

(e) The high-energy nodal dispersion never recovers to the bare dispersion. It remains linear to the highest binding energy studied,[6] with an interpolation to a $\mathbf{k}$ point at zero energy displaced well inside the Fermi surface.

Theoretical scenarios proposed to explain the data differ primarily on whether the electron-electron or the electron-phonon interaction is responsible for the observed behavior. In the electron-electron scenario, the crossover from a linear dispersion at the lowest energies to a more steep dispersion at higher energies has been identified[12] with the crossover from Fermi-liquid to non-Fermi-liquid behavior. In the superconducting state, the *S*-shape dispersion along the antinodal direction has been associated[11,13–15] with the interaction with the (π,π) spin exciton, which below T_c emerges at a

frequency $\omega_{res} < 2\Delta$ due to a feedback of the pairing on the spin susceptibility. The interaction with the exciton gives rise to a $\Sigma'(\omega)$ that strongly increases and then rapidly drops as ω approaches $\omega_0 = \Delta + \omega_{res}$. This gives rise to the observed *S*-shape dispersion. In optimally doped Bi2212, both Δ and ω_{res} are close to 40 meV,[16] i.e., $\omega_0 \sim 80$ meV. The magnitude of the *S*-shape piece is stronger for $|\omega| < \omega_0$, since for $|\omega| > \omega_0$, Σ'' rapidly increases. Both the value of ω_0 and the asymmetry of the *S*-shape dispersion agree with the data.[8,10,11]

For nodal fermions, scattering by $\mathbf{q}_0 = (\pi, \pi)$ shifts the nodal Fermi point to an energy about 0.7 eV above E_F. This energy is too high to expect any appreciable effect on the low-energy dispersion. Still, Eschrig and Norman[15] argued that the kink near 70 meV can be explained by the interaction with the spin resonance, as the resonance has a finite momentum width around (π, π).[17] They used a phenomenological form of the spin susceptibility with a sharp δ function in frequency at ω_{res} and a Lorentzian in momentum space with a width of 2 lattice constants, with the momentum smearing giving rise to resonance scattering between the node and other Fermi surface points. But a good description of the nodal fermion spectrum required the inclusion of a gapped continuum in the spin excitation spectrum, which acts to smear the *S* shape into a kink, and also gives rise to the linear ω behavior in ImΣ observed at higher binding energies.

The electron-phonon scenario for the dispersion was put forward in Ref. 4. The key difference with the electron-electron scenario is in the interpretation of the normal state ARPES data: Ref. 4 argued that there is a sharp kink (rather than a crossover) in the dispersion in the normal state, and that the kink energy is about the same in all materials studied (LSCO, Bi2201, and Bi2212). They further argued that the kink effect is rather isotropic in the Brillouin zone (in disagreement with other work[3,8,10]). They speculated that this similarity implies that superconductivity plays a secondary role in the phenomenon, and that the features in the dispersion can be reproduced by coupling an electron to a bosonic mode unrelated to superconductivity. They suggested a $(\pi, 0)$ optical phonon with an energy of 55 meV (Ref. 18) as the best candidate.

In this paper, we distinguish between these two possibilities and argue in favor of a spin-fluctuation scenario. We first analyze the spin-fluctuation scenario in more detail. We argue that the spin resonance scattering is effective in scattering antinodal fermions near the Fermi energy, but is not effective for nodal fermions since the bosonic momenta which connect a nodal point with other points on the Fermi surface are far removed from (π, π). Rather, the most effective low-energy scattering for a nodal fermion is to the antinode, where the density of states has a singularity. This scattering gives rise to a kink in the self-energy of a nodal fermion at $\sim 2\Delta$, which generates a kink in the dispersion at the same energy. We find that the resonance scattering emerges away from the nodal direction, and the magnitude of the resulting *S*-shape dispersion progressively increases as the antinode is approached.[10]

We then argue that the interaction with an Einstein phonon gives rise to a temperature-independent *S*-shape dispersion for all cuts normal to the Fermi surface. This is difficult to reconcile with both the antinodal dispersion, for which the *S* shape is present but only emerges below T_c, and the nodal dispersion, which does not display an *S*-shape form at any temperature.

II. MAGNETIC SCATTERING

In the magnetic scenario, the fermionic self-energy originates from the strong spin component of the electron-electron interaction in the particle-hole channel and can be viewed as coming from scattering by collective spin fluctuations. To lowest order, the corresponding self-energy is given by

$$\Sigma_{\mathbf{k}_F}(\omega) = -\frac{3ig_s^2}{8\pi^3}\int d^2q\, d\Omega\, G^0_{\mathbf{k}_F+\mathbf{q}}(\omega+\Omega)\chi_s(\mathbf{q},\Omega), \quad (2)$$

where g_s is the spin-fermion coupling. Here G^0 is the bare Green's function (in the normal state, $G^0(\mathbf{k},\omega) = 1/[\omega - v_F(\mathbf{k}_F)(k_\perp - k_F)]$, and $\chi_s(\mathbf{q},\omega)$ is the dynamical spin susceptibility for which one has

$$\chi_s^{-1}(\mathbf{q},\Omega) = \chi_s^{-1}(\mathbf{q}) - \Pi_{\mathbf{q}}(\Omega), \quad (3)$$

where $\chi_s(\mathbf{q})$ is the static part of the susceptibility that is believed to be peaked at or near the antiferromagnetic momentum $\mathbf{q}_0 = (\pi, \pi)$, and $\Pi_{\mathbf{q}}(\Omega)$ [subject to $\Pi_{\mathbf{q}}(0) = 0$] accounts for the spin dynamics and is proportional to the dynamical part of the full particle-hole bubble. For a $\mathbf{q}$ that connects nondiagonal points on the Fermi surface, the polarization operator has the form[19]

$$\Pi_{\mathbf{q}}(\Omega) = i\sum_m \frac{\gamma_{\mathbf{q}}}{2}\int_{-\infty}^{\infty} d\omega \left[1 - \frac{\Delta_+\Delta_- + \omega_+\omega_-}{\sqrt{\omega_+^2 - \Delta_+^2}\sqrt{\omega_-^2 - \Delta_-^2}}\right]. \quad (4)$$

Here $\omega_\pm = \omega \pm \Omega/2$ and $\Delta_\pm = \Delta(\mathbf{k}_m \pm \mathbf{q}/2)$ are the values of the *d*-wave gap at the points $\mathbf{k}_m \pm \mathbf{q}/2$, which are simultaneously on the Fermi surface, the summation *m* being over a discrete set of these points. The prefactor $\gamma_{\mathbf{q}}$ depends on the coupling g_s and the angle between the Fermi velocities at $\mathbf{k}_m \pm \mathbf{q}/2$.[12] In principle, the pairing gap Δ depends on frequency, but this dependence is not essential for our purposes and we neglect it for clarity.

A. Normal state

1. Polarization operator

In the normal state $\Delta = 0$, and $\Pi_{\mathbf{q}}(\Omega)$ is purely imaginary: $\Pi_{\mathbf{q}}(\Omega) = i\gamma_{\mathbf{q}}|\Omega|$. This is the expected result as once $\mathbf{q}$ is such that two $\mathbf{k}$ points separated by $\mathbf{q}$ can be simultaneously put on the Fermi surface, the polarization bubble contains a Landau damping term. This term generally has the form $i|\Omega|/\sqrt{(v_F q)^2 - \Omega^2}$ but in our case q is finite and $v_F q$ well exceeds Ω. The true polarization bubble also contains a frequency-independent piece, but for a finite $\mathbf{q}$, this piece comes from fermions with energies comparable to the bandwidth and is already incorporated into $\chi_s^{-1}(\mathbf{q})$. Note that this separation is consistent with a Kramers-Kronig (KK) analysis: a KK transformation of $\mathrm{Im}\,\Pi(\Omega) = \gamma\Omega$ does not produce

a universal piece of $\mathrm{Re}\,\Pi(\Omega)$ independent of the upper limit of the frequency integration.

2. Fermionic self-energy

Substituting the relaxational $\chi_s(\mathbf{q},\Omega)$ into the self-energy, introducing a small $\mathbf{q}$ via $\mathbf{q}\to\mathbf{q}+\mathbf{q}_0$ and linearizing the fermionic dispersion near the Fermi surface, we obtain from Eq. (2)

$$\Sigma_{N,\mathbf{k}_F}(\omega) = -i\frac{3g_s^2}{8\pi^3}\int dq_{\|}dq_{\perp}d\Omega \times\frac{1}{\omega+\Omega-v_F(\mathbf{k}_F+\mathbf{q}+\mathbf{q}_0)q_{\perp}+i\delta_{\omega+\Omega}} \times\frac{1}{\chi_s^{-1}(\mathbf{q}+\mathbf{q}_0)-i\gamma_{\mathbf{q}+\mathbf{q}_0}|\Omega|}, \tag{5}$$

where N stands for normal state. For consistency with the assumption that the self-energy weakly depends on $\epsilon_{\mathbf{k}}$, we assume that the fermionic propagator changes much faster with $q_{\perp}$ than the bosonic $\chi(\mathbf{q},\Omega)$, i.e., that the Fermi velocity is much larger than the "spin" velocity. We then integrate over momentum $q_{\perp}$ normal to the Fermi surface only in the fermionic propagator, and set $q_{\perp}$ in the bosonic propagator equal to its value at a distance between $\mathbf{k}_F$ and some other point on the Fermi surface, which is parametrized by $q_{\|}$. The integration over $q_{\perp}$ is straightforward, and performing it using the fact that $\chi_s(\mathbf{q},\Omega)$ is an even function of frequency, we obtain

$$\Sigma_{N,\mathbf{k}_F}(\omega) = -\frac{3g_s^2}{4\pi^2}\int dq_{\|}\frac{1}{v_F(\mathbf{k}_F+\mathbf{q}_0+\mathbf{q}_{\|})} \times\int_0^{\omega}\frac{d\Omega}{\chi_s^{-1}(\mathbf{q}_0+\mathbf{q}_{\|})-i\gamma_{\mathbf{q}_0+\mathbf{q}_{\|}}\Omega}. \tag{6}$$

The remaining integral over $q_{\|}$ depends on the momentum dispersions in $\chi_s(\mathbf{q})$ and $v_F(\mathbf{k}_F)$ along the Fermi surface, both are inputs for the low-energy theory. For a qualitative understanding of the crossover in the dispersion, we assume momentarily that $\chi_s(\mathbf{q}_0+\mathbf{q}_{\|})$ is flat near $\mathbf{q}_0$, and that $\gamma_{\mathbf{q}_0+\mathbf{q}_{\|}}$ and $v_F(\mathbf{k}_F+\mathbf{q}_0+\mathbf{q}_{\|})$ are also momentum independent. We then immediately obtain from Eq. (6)

$$\Sigma_{N,\mathbf{k}_F}(\omega) = -i\lambda\omega_{sf}\ln\left[1-\frac{i|\omega|}{\omega_{sf}}\right]\mathrm{sgn}(\omega), \tag{7}$$

where $\lambda=3g_s^2\chi_s/(2\pi v_F)$ and $\omega_{sf}=(\chi_s\gamma)^{-1}$ (we use the same notation as in earlier works[12,20]). Separating real and imaginary parts of the complex logarithm, we obtain from Eq. (6)

$$\mathrm{Re}\,\Sigma_{N,\mathbf{k}_F}(\omega) = -\lambda\omega_{sf}\arctan\frac{\omega}{\omega_{sf}},$$

$$\mathrm{Im}\,\Sigma_{N,\mathbf{k}_F}(\omega) = -\lambda\frac{\omega_{sf}}{2}\ln\left[1+\frac{\omega^2}{\omega_{sf}^2}\right]\mathrm{sgn}(\omega). \tag{8}$$

At low frequencies, one indeed recovers Fermi-liquid behavior:[21]

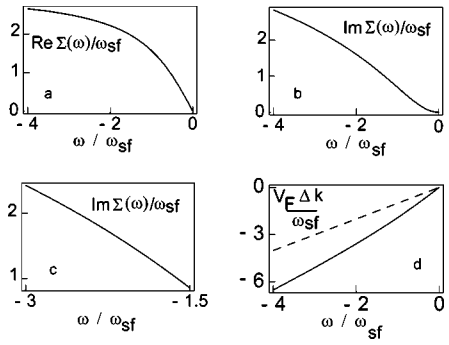

FIG. 1. The self-energy and the dispersion in the normal state for a flat static susceptibility $\chi_s(\mathbf{q})$ near $\mathbf{q}_0=(\pi,\pi)$. (a) $\mathrm{Re}\,\Sigma_N$, (b) and (c) $\mathrm{Im}\,\Sigma_N$, with (c) over intermediate frequencies where $\mathrm{Im}\,\Sigma_N(\omega)$ displays a quasilinear behavior. (d) Dispersion $\omega-\mathrm{Re}\,\Sigma(\omega)=v_F\Delta k$ ($\Delta k=k-k_F$), with the dashed line the free fermion dispersion. The coupling is $\lambda=2$.

$$\Sigma_{N,\mathbf{k}_F}(\omega) = -\lambda\left(\omega+i\frac{\omega|\omega|}{2\omega_{sf}}\right). \tag{9}$$

On the other hand, at frequencies larger than ω_{sf}, the self-energy nearly saturates:

$$\Sigma_N'(\omega)\approx-(\pi/2)\lambda\omega_{sf}\,\mathrm{sgn}(\omega),\quad \Sigma_N''(\omega)\propto\ln|\omega|. \tag{10}$$

The evolution of $\Sigma_N'(\omega)$ with frequency gives rise to a crossover in the normal state dispersion $\omega-\Sigma_N'(\omega)=v_F(k_{\perp}-k_F)$ around $\omega=\omega_{sf}$. We illustrate this in Fig. 1. We clearly see that the dispersion is linear below ω_{sf}, with the effective velocity $v_F^*=v_F/(1+\lambda)$. However, above ω_{sf}, the dispersion crosses over to a more steep form, which also yields an intercept at a finite $k_{\perp}-k_F$ if extrapolated formally to zero energy. This crossover behavior is consistent with the one observed experimentally. Note also that $\Sigma_N''(\omega)$ is almost linear in frequency in a relatively wide frequency range above ω_{sf}. This quasilinearity seems to be a generic property of Σ_N'' in the crossover region between ω^2 Fermi liquid behavior at small frequencies and quantum-critical, non-Fermi-liquid behavior at larger frequencies.

The inclusion of the momentum dependences of $\chi_s(\mathbf{q})$, $\gamma_{\mathbf{q}}$, and $v_F(\mathbf{k}_F)$ gives rise to some ω dependence of $\Sigma_N'(\omega)$ at high frequencies, and to the angular dependence of the coupling constant λ, but the crossover near ω_{sf} still survives. To illustrate this, in Fig. 2 we plot the the dispersion obtained for the Ornstein-Zernike form of $\chi_s^{-1}(\mathbf{q})\propto1+(q\xi)^2$ with constant γ and v_F. We see that the dispersion is again linear at small ω with $v_F^*=v_F/(1+\lambda_{\mathbf{k}_F})$, and crosses over to a more steep dispersion above $\omega_{sf}(\mathbf{k}_F)$. Observe also that $\Sigma''(\omega)$ is again nearly linear above $\omega_{sf}(\mathbf{k}_F)$. The crossover frequency $\omega_{sf}(\mathbf{k}_F)=[\gamma\chi_s(\mathbf{k}_F)]^{-1}$ is smallest for an antinodal fermion and largest for a nodal fermion simply because the node-node distance is smaller than $\mathbf{q}_0=(\pi,\pi)$, and hence for node-node scattering $\chi_s^{-1}(\mathbf{q})\propto[1+(|\mathbf{q}-\mathbf{q}_0|\xi)^2]$. For an antinodal fermion, on the other hand, the antinode-antinode scattering involves momenta very close to $\mathbf{q}_0$, hence $\chi_s^{-1}(\mathbf{q})$ is smaller as the piece $(|\mathbf{q}-\mathbf{q}_0|\xi)^2$ is absent. This effect is, however, partly compensated by the fact that $\gamma_{\mathbf{q}}$ is enhanced around a

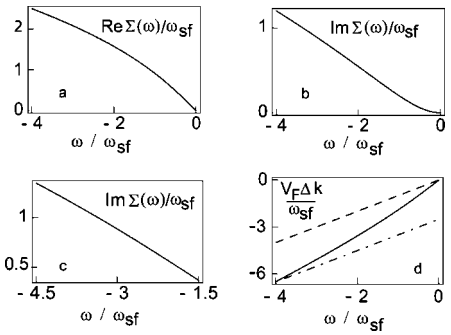

FIG. 2. Same as Fig. 1, but for the Ornstein-Zernike form of the static spin susceptibility and $\lambda=1$. In both cases, the crossover occurs around $\omega=\omega_{sf}$. The dashed line in (d) is the free-fermion dispersion. The dashed-dotted line in (d) is an extrapolation from high frequencies. The extrapolated dispersion crosses the vertical axis at a negative Δk, i.e., for k inside the Fermi surface.

nodal point and formally diverges for node-node scattering because the Landau damping blows up when the velocities of the two fermions in the particle-hole bubble become antiparallel to each other, as is the case for nodal fermions.[22] Previous calculations show[22] that, as an interplay between the two effects, the variation of ω_{sf} along the Fermi surface near optimal doping is relatively modest, i.e, the crossover frequency for the normal state does not vary substantially along the Fermi surface.

B. Superconducting state

1. Polarization operator

We begin with the polarization operator, Eq. (4). Applying the spectral representation to Eq. (4), one can immediately see that in the superconducting state, $\mathrm{Im}\,\Pi_{\mathbf{q}}(\Omega)$ remains linear in frequency only for $\Omega \gg \Delta$ [where $\mathrm{Im}\,\Pi_{\mathbf{q}}(\Omega)=\gamma\Omega$]. At smaller frequencies, $\mathrm{Im}\,\Pi_{\mathbf{q}}(\Omega)$ vanishes below a threshold at $\Omega_{th}=|\Delta_+|+|\Delta_-|$, where, we remind, $\Delta_\pm=\Delta(\mathbf{k}_m\pm\mathbf{q}/2)$, and $\mathbf{k}_m+\mathbf{q}/2$ and $\mathbf{k}_m-\mathbf{q}/2$ are discrete pairs of momenta (specified by m), which are simultaneously on the Fermi surface. By the Kramers-Kronig relation, the vanishing of $\mathrm{Im}\,\Pi_{\mathbf{q}}(\Omega)$ below the threshold generates a nonzero $\mathrm{Re}\,\Pi_{\mathbf{q}}(\Omega)$, which comes from frequencies of order Δ and is therefore part of the low-energy theory. This $\mathrm{Re}\,\Pi_{\mathbf{q}}(\Omega)$ dominates the spin dynamics below the threshold.

The structure of $\Pi_{\mathbf{q}}(\Omega)$ in a d-wave superconductor has been previously analyzed for $\mathbf{q}=\mathbf{q}_0=(\pi,\pi)$.[23] For $\mathbf{q}=\mathbf{q}_0$, different regions specified by m are all equivalent, $\Delta(\mathbf{k}_F+\mathbf{q}_0)=-\Delta(\mathbf{k}_F)=\Delta$, i.e., $\Omega_{th}=2\Delta$. At the threshold frequency, $\mathrm{Im}\,\Pi_{\mathbf{q}_0}(\Omega)$ is discontinuous and jumps from zero to $\pi\Delta\gamma$. By the KK relation, $\mathrm{Re}\,\Pi_{\mathbf{q}_0}(\Omega)$ then diverges logarithmically at Ω_{th}.[14] This divergence ensures that for arbitrary coupling, $\chi_s(\mathbf{q},\Omega)=[\chi_s^{-1}(\mathbf{q})-\Pi_{\mathbf{q}}(\Omega)]^{-1}$ has an excitonic pole at some $\omega_{res}<2\Delta$, where $\Pi_{\mathbf{q}_0}(\omega_{res})=\mathrm{Re}\,\Pi_{\mathbf{q}_0}(\omega_{res})=\chi_s^{-1}$. At weak coupling, ω_{res} is exponentially close to 2Δ, and the resonance is easily washed out by, e.g., disorder. At strong coupling, however, the pole is located at small frequencies and is weakly affected by disorder. Furthermore, expanding Eq. (4) in powers of Ω, one can easily find that at the lowest frequencies, $\Pi_{\mathbf{q}_0}(\Omega)\propto\Omega^2/\Delta$, i.e., at strong coupling, when $\omega_{res}\ll 2\Delta$, the low-frequency spin susceptibility has a magnonlike form $\chi_s(\mathbf{q}_0,\Omega)\propto(\omega_{res}^2-\Omega^2)^{-1}$.

The resonance behavior of $\Pi_{\mathbf{q}_0}(\Omega)$ sets the crossover in the dispersion of an antinodal fermion, for which the scattering by $\mathbf{q}_0$ is a low-energy process. For a nodal fermion, however, the scattering by $\mathbf{q}_0$ is ineffective, and one should analyze other $\mathbf{q}$.[15] For a general $\mathbf{q}\neq\mathbf{q}_0$ connecting two Fermi-surface points, we find from Eq. (4) that the magnitude of the jump in $\mathrm{Im}\,\Pi_{\mathbf{q}}(\Omega)$ at the threshold frequency $\Omega_{th}=|\Delta(\mathbf{k}_F)|+|\Delta(\mathbf{k}_F+\mathbf{q})|$ is

$$\delta(\mathrm{Im}\,\Pi_{\mathbf{q}}(\Omega_{th}))=\frac{\pi\gamma}{2}\sqrt{|\Delta(\mathbf{k}_F)\Delta(\mathbf{k}_F+\mathbf{q})|}\times\{1-\mathrm{sgn}[\Delta(\mathbf{k}_F)\Delta(\mathbf{k}_F+\mathbf{q})]\}. \quad (11)$$

It then follows that for scattering from a nodal Fermi surface point $\mathbf{k}_{F,n}$ to some other point $\mathbf{k}_F=\mathbf{k}_{F,n}+\mathbf{q}$ along the Fermi surface, the jump in $\mathrm{Im}\,\Pi_{\mathbf{q}}(\Omega_{th})$ disappears because $\Delta(\mathbf{k}_{F,n})=0$, even though $\Delta(\mathbf{k}_{F,n}+\mathbf{q})\neq 0$. In the absence of a jump in $\mathrm{Im}\,\Pi_{\mathbf{q}}(\Omega)$ at Ω_{th}, $\mathrm{Re}\,\Pi_{\mathbf{q}}(\Omega)$ does not diverge when approaching Ω_{th} from below. Indeed, by the KK relation

$$\mathrm{Re}\,\Pi_{\mathbf{q}}(\Omega)=\frac{2}{\pi}\int_0^\infty\frac{dx\,\mathrm{Im}\,\Pi_{\mathbf{q}}(x)}{x^2-\Omega^2}. \quad (12)$$

Near $\Omega=\Omega_{th}$, this reduces to

$$\mathrm{Re}\,\Pi_{\mathbf{q}}(\Omega)\approx\frac{1}{\pi\Omega_{th}}\int_0^\infty\frac{dy\,\mathrm{Im}\,\Pi_{\mathbf{q}}(y+\Omega_{th})}{y+(\Omega_{th}-\Omega)}. \quad (13)$$

When $\mathrm{Im}\,\Pi_{\mathbf{q}}(\Omega_{th}+0^+)$ has a nonzero value [which is the case when $\mathrm{Im}\,\Pi_{\mathbf{q}}(\Omega)$ jumps at the threshold], it can be pulled out from the integral over y, and $\mathrm{Re}\,\Pi_{\mathbf{q}}(\Omega_{th})$ diverges logarithmically. Without the jump, $\mathrm{Im}\,\Pi_{\mathbf{q}}(y+\Omega_{th})$ vanishes at $y=0^+$, and the integral over y in relation (13) does not diverge. We find from Eq. (4) that for scattering that involves a nodal fermion, $\mathrm{Im}\,\Pi_{\mathbf{q}}(y+\Omega_{th})\propto y^{1/2}$, hence for $\Omega<\Omega_{th}$ we have from Eq. (13),

$$\mathrm{Re}\,\Pi_{\mathbf{q}}(\Omega)=-\gamma\sqrt{\Omega_{th}^2-\Omega^2}. \quad (14)$$

The minus sign in front of the square-root implies that $\mathrm{Re}\,\Pi_{\mathbf{q}}(\Omega)$ is negative, i.e., $\chi^{-1}(\mathbf{q},\Omega)=\chi_s^{-1}(\mathbf{q})-\Pi_{\mathbf{q}}(\Omega)$ does not change sign below Ω_{th}, and the resonance mode does not emerge. We recall that a constant, Δ independent term, has been already pulled out from $\mathrm{Re}\,\Pi_{\mathbf{q}}(\Omega)$, hence the negative value is with respect to the normal state [as $\chi_s^{-1}(\mathbf{q})>0$ in a paramagnet, $\chi_s^{-1}(\mathbf{q})-\Pi_{\mathbf{q}}(\Omega)$ is positive for all $\Omega<\Omega_{th}$].

Equation (14) can be easily extended to the full complex $\Pi_{\mathbf{q}}(\Omega)$, which takes the form

$$\Pi_{\mathbf{q}}(\Omega)=i\gamma\sqrt{(\Omega+i\delta)^2-\Omega_{th}^2}. \quad (15)$$

Note that the square-root functional form of $\Pi_{\mathbf{q}}(\Omega)$ survives even when the scattering is between a nodal fermion and a point not exactly on the Fermi surface. Indeed, as long as $\mathbf{q}$ is not directed along the zone diagonal, one can set, without loss of generality, the velocity of a nodal fermion to be along

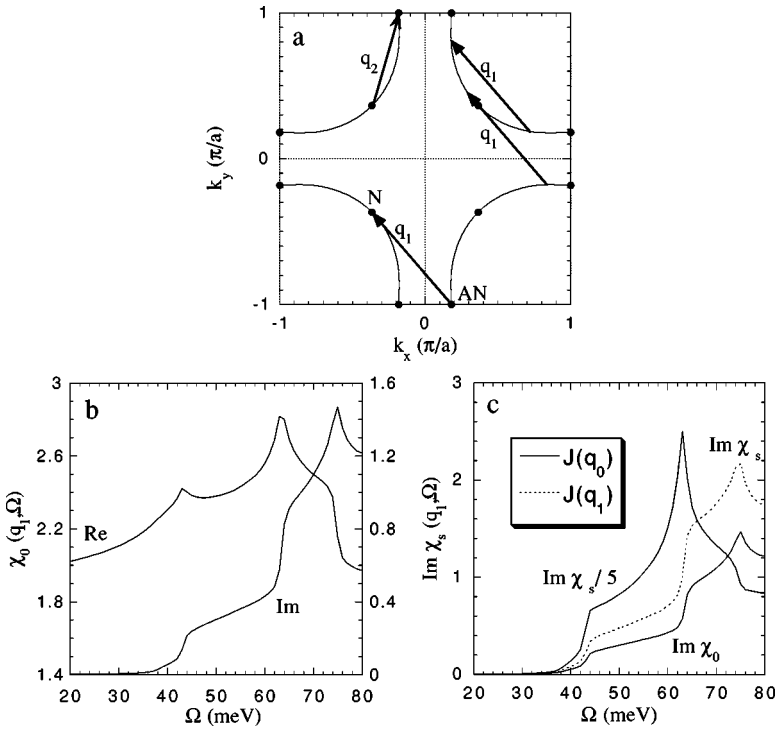

FIG. 3. (a) Different pairs of Fermi surface points separated by a momentum $\mathbf{q}_1$ equal to the node-antinode distance. Solid points mark the node (N) and antinode (AN). In addition, the other node-antinode wavevector ($\mathbf{q}_2$) is shown. (b) The imaginary and real parts of the particle-hole bubble $\chi_0(\mathbf{q}_1,\Omega)$. The spin polarization operator $\Pi(\mathbf{q},\Omega)=\chi_0^{-1}(\mathbf{q},0)-\chi_0^{-1}(\mathbf{q},\Omega)$. Note near discontinuities in Im χ_0 at $\Omega'_{th}\approx 1.07\Delta$ and 1.6Δ. Here, $\Delta_{(\pi,0)}=40$ meV, $\delta=0.5$ meV, and $T=0.5$ meV. (c) Im $\chi_s(\mathbf{q}_1,\Omega)$ for two values of $J(\mathbf{q})$ [$\chi_s^{-1}(\mathbf{q})=\chi_0^{-1}(\mathbf{q},0)-J(\mathbf{q})$]. Here, $J(\mathbf{q}_0)$ was chosen so as to yield a resonance at 40 meV for $\mathbf{q}=\mathbf{q}_0$, and $J(\mathbf{q}_1)$ is $-J(\mathbf{q}_0)[\cos(q_{1x}a)+\cos(q_{1y}a)]/2$.

the y axis, i.e., $\epsilon_{\mathbf{k}}=y$, and the velocity of a fermion at $\mathbf{k}+\mathbf{q}$ to be along x: $\epsilon_{\mathbf{k}+\mathbf{q}}=\epsilon_0+x$ where $\epsilon_0=\epsilon_{\mathbf{k}_F+\mathbf{q}}$. Substituting this expansion into $\Pi_{\mathbf{q}}(\Omega)\propto\int G_{\mathbf{k},\omega+\Omega}G_{\mathbf{k}+\mathbf{q},\omega}$ we obtain

$$\Pi_{\mathbf{q}}(\Omega)\propto\int d\omega\frac{dxdy}{\omega+\Omega-y+i\delta_{\omega+\Omega}}\times\frac{\epsilon_0+x+\omega}{\omega^2-(\epsilon_0+x)^2-\Delta^2(x,y)+i\delta}. \quad (16)$$

Elementary analysis shows that the singular contribution to $\Pi_{\mathbf{q}}(\Omega)$ comes from $\omega=-\Omega$, $y=0$, and $x=-\epsilon_0$, i.e., from the internal momentum range when both fermions are back on the Fermi surface. Furthermore, as typical y are infinitesimally small, one can neglect the y dependence of the gap, in which case the momentum integral is factorized. Integrating over y, then over ω, and finally over x, one immediately recovers Eq. (15) with $\Omega_{th}=\Delta(-\epsilon_0,0)$, that is, the gap at the Fermi surface point obtained by projecting $\mathbf{k}+\mathbf{q}$ onto the Fermi surface along the x direction.

The square-root behavior of $\Pi_{\mathbf{q}}(\Omega)$ is not the full story, however, as the same incommensurate $\mathbf{q}$ which connects a nodal Fermi surface point with some other $\mathbf{k}_F$ may also connect other pairs of Fermi surface points for which the superconducting gap is nonzero for both points. If the signs of the two gaps are opposite, then, according to Eq. (11), Im $\Pi_{\mathbf{q}}(\Omega)$ still has discontinuities at the corresponding threshold frequencies Ω'_{th}, hence Re $\Pi_{\mathbf{q}}(\Omega'_{th})$ diverges, and $\chi_s^{-1}(\mathbf{q})-\mathrm{Re}\,\Pi_{\mathbf{q}}(\Omega)$ crosses zero at some frequency below Ω'_{th}. We checked this possibility for the Fermi surface of optimally doped Bi2212.[23] For node-antinode scattering, there are two inequivalent $\mathbf{q}$ vectors. The smaller of the two, which we label $\mathbf{q}_2$, has a dynamic response that is small relative to the larger of the two, which we label $\mathbf{q}_1$. For $\mathbf{q}_1$, the node-antinode process at the $\Omega=\Delta_{an}$ is the threshold for Im $\Pi_{\mathbf{q}_1}(\Omega)$ (an=antinode). There are, though, two other inequivalent pairs of vectors for which $\mathbf{k}$ and $\mathbf{k}+\mathbf{q}_1$ are both on the Fermi surface, and $\Delta(\mathbf{k})$ and $\Delta(\mathbf{k}+\mathbf{q}_1)$ have opposite signs. For these processes, Im $\Pi_{\mathbf{q}}(\Omega)$ is discontinuous at corresponding threshold frequencies $\Omega'_{th}\approx 1.07\Delta$ and 1.6Δ. We illustrate this in Fig. 3. We found, however, that these extra processes do not give rise to a resonance in the spin susceptibility for two reasons. First, the dynamic response at $\mathbf{q}_1$ is weaker than that at $\mathbf{q}_0$, and the divergence in Re $\Pi_{\mathbf{q}_1}$ is further weakened at the lower energy Ω'_{th} of the two since one of the two $\mathbf{k}$ vectors is near the node in this case. Thus, the inclusion of any damping (due to impurities or finite T) is enough to remove the divergence altogether. Second, even in an idealized situation with zero fermionic damping, the threshold frequencies Ω'_{th} for both of these extra scattering processes exceed Ω_{th}, hence near Ω'_{th}, Im $\Pi_{\mathbf{q}_1}(\Omega)$ is already nonzero. As a consequence, we find no resonance for Im $\chi_s(\mathbf{q}_1,\Omega)$ (though there can be a peak associated with the higher energy Ω'_{th}).

Summarizing, we argue that for $\mathbf{q}_1$, which connects nodal and antinodal Fermi surface points, there is no actual resonance in the spin susceptibility. The imaginary part of $\chi_s(\mathbf{q},\Omega)$ emerges at $\Omega_{th}=\Delta_{an}$ as $(\Omega-\Delta_{an})^{1/2}$ and has extra bumps at higher energies near threshold frequencies for additional scattering processes with the same $\mathbf{q}$. Alternatively speaking, the excitonic resonance in the dynamical spin susceptibility exists for $\mathbf{q}$ near $\mathbf{q}_0$ but gradually vanishes as $\mathbf{q}$ approaches $\mathbf{q}_1$. The boundary between these two regions is roughly set by the diagonal node-node scattering vector, which has a length intermediate between $\mathbf{q}_0$ and $\mathbf{q}_1$.

2. Fermionic self-energy

We next compute the fermionic self-energy, Eq. (2). For an antinodal fermion, both $\mathbf{k}$ and $\mathbf{k}+\mathbf{q}_0$ are near the Fermi

surface, and the resonance mode has a strong effect on the self-energy. Assuming that $\chi_s(\mathbf{q},\Omega)$ has a magnonlike form $\chi_s(\mathbf{q},\Omega)=\chi_0/[\omega_{res}^2(\mathbf{q})-\Omega^2]$, adding a small damping term $i\delta$ to Ω for continuity, and neglecting the momentum dependence of ω_{res} both for simplicity and because experimentally, the resonance dispersion is rather flat,[24] we obtain from Eq. (2) in the superconducting state

$$\Sigma_{SC,an}(\omega)=\frac{3ig_s^2\chi_0}{4\pi^2 v_F}\int\frac{dxd\Omega(\omega+\Omega+x)}{x^2+\Delta^2-(\omega+\Omega)^2-i\delta}\times\frac{1}{\omega_{res}^2-\Omega^2-i\delta}. \quad (17)$$

The subscript for the self-energy implies SC =superconducting state, an=antinode. We also defined $x=v_F q_\perp$ and used the superconducting Green's function for free fermions:

$$G_{SC}^0(\mathbf{k},\omega)=\frac{\omega+\epsilon_{\mathbf{k}}}{\omega^2+i\delta-\Delta^2-\epsilon_{\mathbf{k}}^2}. \quad (18)$$

The integration over x is straightforward, and performing it we obtain

$$\Sigma_{SC,an}(\omega)=-\frac{3g_s^2\chi_0}{4\pi v_F}\int\frac{d\Omega}{\omega_{res}^2-\Omega^2-i\delta}\times\frac{\omega+\Omega}{\sqrt{(\omega+\Omega)^2-\Delta^2+i\delta}}. \quad (19)$$

This integral is singular near $\omega=-\omega_0=-(\Delta+\omega_{res})$. To see this, introduce $\omega=-\omega_0+\epsilon$, and $\Omega=\omega_{res}+y$. Substituting these expansions into Eq. (19) and restricting to only linear terms in y and ϵ, we obtain after simple algebra

$$\Sigma_{SC,an}(\epsilon)=-\frac{3g_s^2\chi_0\sqrt{\Delta}}{8\pi\sqrt{2}\omega_{res}v_F}\int\frac{dy}{y+i\delta}\frac{1}{\sqrt{-\epsilon-y+i\delta}}. \quad (20)$$

Splitting the integration over y into integrals over positive and negative y and evaluating them separately, we obtain

$$\int_{-\infty}^{\infty}\frac{dy}{y+i\delta}\frac{1}{\sqrt{-\epsilon-y+i\delta}}=-\frac{2\pi}{\sqrt{\epsilon-i\delta}}. \quad (21)$$

Substituting this into Eq. (20) we obtain

$$\Sigma_{SC,an}(\epsilon)=\frac{3g_s^2\chi_0\sqrt{\Delta}}{8\omega_{res}v_F}\frac{\sqrt{2}}{\sqrt{\epsilon-i\delta}}. \quad (22)$$

Separating real and imaginary parts of $1/\sqrt{\epsilon-i\delta}$ and replacing ϵ back by $\omega+\omega_0$ we finally obtain

$$\Sigma'_{SC,an}(\omega)=\lambda_{eff}\Delta^{3/2}\frac{(\omega+\omega_0+\sqrt{(\omega_0+\omega)^2+\delta^2})^{1/2}}{\sqrt{(\omega_0+\omega)^2+\delta^2}}, \quad (23)$$

where

$$\lambda_{eff}=\frac{3g_s^2\chi_0}{8v_F\Delta^2}\frac{\Delta}{\omega_{res}}. \quad (24)$$

Note that λ_{eff} is dimensionless (with the above definition of χ_0).

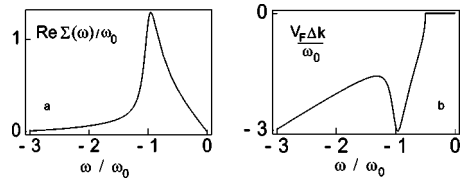

FIG. 4. The self-energy and the dispersion near an antinodal point. The coupling is $\lambda(\mathbf{q}_1)=2$. We also set $\Delta=\omega_{res}$, i.e., $\omega_0=2\Delta$, and use a broadening $\delta=0.3\Delta$. Note the *S*-shape dispersion near ω_0.

We see from Eq. (23) that the real part of the self-energy has a near one-sided singularity. It almost diverges as $1/\sqrt{\omega_0+\omega}$ as ω approaches $-\omega_0$ from above ($|\omega|<\omega_0$), and then rapidly drops beyond $-\omega_0$, reducing to $O(\delta^2/(\omega+\omega_0))$ when $|\omega|>\omega_0$. The relation between this self-energy and the dispersion is somewhat complicated in a superconductor, as the MDC line shape does not have a simple Lorentzian form because the Green's function has $\epsilon_{\mathbf{k}}=v_F(k_\perp-k_F)$ both in the numerator and the denominator:

$$G(\mathbf{k},\omega)=\frac{\omega-\Sigma(\omega)+\epsilon_{\mathbf{k}}}{[\omega-\Sigma(\omega)]^2-\Phi^2(k_\parallel,\omega)-\epsilon_{\mathbf{k}}^2}. \quad (25)$$

Here $\Phi(k_\parallel,\omega)$ is the pairing vertex. It is related to the pairing gap $\Delta(k_\parallel,\omega)$ by $\Phi(k_\parallel,\omega)=\Delta(k_\parallel,\omega)Z(\omega)$, where $Z(\omega)=1-\Sigma(\omega)/\omega$.[15,19,25] For simplicity, we neglect the frequency dependence of $\Delta(k_\parallel,\omega)$, i.e., approximate $\Delta(k_\parallel,\omega)$ by a frequency-independent gap $\Delta(k_\parallel)$. Near the antinodal points, the gap is near its maximum, i.e., is rather flat as a function of $k_\parallel$, and can be approximated by a constant Δ. Still, the presence of $\epsilon_{\mathbf{k}}$ in the numerator of Eq. (25) implies that the maximum of $\mathrm{Im}\,G(\mathbf{k},\omega)$ is shifted somewhat in ω from where the real part of the the denominator in Eq. (25) vanishes (in the BCS limit, this effect can be attributed to the k dependence of the coherence factors). This complication, however, affects the form of the dispersion mainly for $|\omega|<\Delta$, and is less relevant near $\omega=-\omega_0$ where the self-energy is nearly singular. To avoid this complication, we neglect the k dependence of the numerator of the Green's function, and extract the dispersion from

$$\mathrm{Re}[\omega-\Sigma(\omega)+\sqrt{\Phi^2(\omega)+v_F^2(k_\perp-k_F)^2}]=0. \quad (26)$$

Substituting $\Phi(\omega)$ in terms of Δ, and neglecting $\mathrm{Im}\,Z(\omega)$ (which vanishes for $|\omega|<\omega_0$ anyway), we obtain from Eq. (26)

$$[\omega-\Sigma'_{SC,an}(\omega)]\mathrm{Re}\sqrt{\frac{\omega^2-\Delta^2}{\omega^2}}=v_F(k_\perp-k_F). \quad (27)$$

Substituting $\Sigma'_{SC,an}$ from Eq. (23), we find that the dispersion develops an *S* shape for $|\omega|<\omega_0$, precisely as seen in the experiments. We illustrate this in Fig. 4. We also recall that a near divergence of $\mathrm{Re}\,\Sigma_{an}(\omega_0)$ implies, by KK transform, a near discontinuity in $\mathrm{Im}\,\Sigma_{an}(\omega_0)$, both of which give rise to the experimentally observed peak/dip/hump behavior of the ARPES intensity.[13,16]

For a nodal fermion, the situation is different. A shift by $\mathbf{q}_0$ moves a nodal Fermi surface point to a point where the energy is very large, ~ 0.7 eV for optimally doped Bi2212. The (π,π) scattering is then ineffective. However, for $\mathbf{q}$ that we analyzed in the preceding section, a nodal fermion can still scatter along the Fermi surface, which gives rise to a much larger self-energy.

The computation of the self-energy $\Sigma_{SC,n}(\omega)$ requires extra care, as we will have to average over all $\mathbf{q}$ that connect a nodal point with other points on the Fermi surface. Besides, even for the integration near a particular $\mathbf{q}$, the dispersion of the *d*-wave gap is essential as it affects the functional form of $\mathrm{Im}\,\Sigma_{SC,n}(\omega)$ via the softening of the singularity in the fermionic density of states at fermionic frequencies near the gap at $\mathbf{k}_F+\mathbf{q}$. As our goal is to demonstrate that the self-energy at the nodal point does not have the sharp features of the antinodal self-energy, we assume for simplicity that (i) the dominant contribution to $\Sigma_{SC,n}(\omega)$ comes from node-antinode scattering, because of the presence of the density of states singularity associated with the antinode, and (ii) that the superconducting gap has a flat dispersion in the antinode region.

Substituting the spin susceptibility with Π given by Eq. (15) into Eq. (2) and neglecting momentarily the dispersion in $\chi_s(\mathbf{q})$ around $\mathbf{q}_1$, we obtain after integrating over momentum near the Fermi surface ($\Omega_{th}=\Delta$)

$$\Sigma_{SC,n}(\omega)=\frac{\lambda(\mathbf{q}_1)}{2}\int_{-\infty}^{\infty}d\omega'\frac{\omega'}{\sqrt{(\omega')^2-\Delta^2}}\times\frac{1}{1-i\sqrt{(\omega+\omega')^2-\Delta^2}/\omega_{sf}(\mathbf{q}_1)}, \tag{28}$$

where $\omega_{sf}(\mathbf{q}_1)=[\gamma_{\mathbf{q}_1}\chi_s(\mathbf{q}_1)]^{-1}$. At the lowest frequencies, expanding to linear order in ω and collecting the prefactor, we obtain

$$\mathrm{Re}\,\Sigma_{SC,n}(\omega)=-\lambda_{sc}(\mathbf{q}_1)\omega, \tag{29}$$

where $\lambda_{sc}(\mathbf{q}_1)=\lambda(\mathbf{q}_1)\psi(\Delta/\omega_{sf}(\mathbf{q}_1))$, and

$$\psi(x)=\int_0^{\infty}\frac{dz}{(z^2+1)^{3/2}}\frac{1}{1+x\sqrt{z^2+1}} \tag{30}$$

such that $\psi(x)\leqslant\psi(0)=1$. This implies that the coupling constant in the superconducting state is somewhat smaller than in the normal state. This is in agreement with earlier work.[12] At larger frequencies, $\mathrm{Re}\,\Sigma_{SC,n}(\omega)$ is continuous and reduces to its nearly flat normal state form, Eq. (10), at $|\omega|\gg\Delta,\omega_0$. The limiting behavior resembles that in the normal state; however, the crossover in Eq. (28) is not analytic, and the self-energy develops a kink at $\omega=-2\Delta$. This can be most easily seen by evaluating the derivative of the self-energy. Indeed, differentiating with respect to ω in Eq. (28), we obtain

$$\frac{d\Sigma_{SC,n}(\omega)}{d\omega}=\frac{i\lambda(\mathbf{q}_1)}{2\omega_{sf}(\mathbf{q}_1)}\int\frac{d\omega'}{\sqrt{(\omega')^2-\Delta^2}\sqrt{(\omega+\omega')^2-\Delta^2}}\times\frac{\omega'(\omega+\omega')}{[1-i\sqrt{(\omega+\omega')^2-\Delta^2}/\omega_{sf}(\mathbf{q}_1)]^2}. \tag{31}$$

Near $\omega=\pm 2\Delta$, the dominant contribution to the integral comes from $\omega'\approx-\Delta\,\mathrm{sgn}(\omega)$, when the two branch-cut singularities merge. In this region, $\omega'(\omega+\omega')\approx-\Delta^2$, $(\omega+\omega')^2\approx\Delta^2$, and

$$\frac{d\Sigma_{SC,n}(\omega)}{d\omega}\approx\frac{-i\lambda(\mathbf{q}_1)\Delta^2}{2\omega_{sf}(\mathbf{q}_1)}\int\frac{d\omega'}{\sqrt{(\omega')^2-\Delta^2}\sqrt{(\omega+\omega')^2-\Delta^2}}. \tag{32}$$

Evaluating the integral, we find that at, e.g., $\omega=-2\Delta$, $d\,\mathrm{Im}\,\Sigma(\omega)/d\omega$ undergoes a finite jump

$$\frac{d}{d\omega}[\mathrm{Im}\,\Sigma_{SC,n}(-2\Delta-\epsilon)-\mathrm{Im}\,\Sigma_{SC,n}(-2\Delta+\epsilon)]\propto\int_0^{\epsilon}\frac{dx}{\sqrt{x}\sqrt{\epsilon-x}}=2\int_0^1\frac{dz}{\sqrt{1-z^2}}=\pi. \tag{33}$$

By the KK relation, $d\,\mathrm{Re}\,\Sigma(\omega)/d\omega$ diverges logarithmically at $\omega=-2\Delta$. This behavior is analogous to the behavior of the polarization operator with $\mathbf{q}=(\pi,\pi)$ near the threshold frequency $\Omega_{th}=2\Delta$. Evaluating $d\Sigma'_{SC,n}(\omega)/d\omega$ explicitly, introducing $\omega=-2\Delta+\epsilon$ and $\omega'=\Delta+x$, and expanding to first order in x and in ϵ in the two terms in the denominator, we obtain near $\omega=-2\Delta$

$$\frac{d\Sigma'_{SC,n}(\omega)}{d\omega}\approx\frac{\lambda(\mathbf{q}_1)\Delta}{4\omega_{sf}(\mathbf{q}_1)}\,\mathrm{Im}\left[\int_{-A}^{A}\frac{dx}{\sqrt{x+i\delta}\sqrt{-\epsilon-x+i\delta}}\right]. \tag{34}$$

Here $A\sim\Delta$ is the upper cutoff for the linear expansion. Splitting the integral into the integrals over positive x and over negative x, and evaluating them separately, we obtain, to logarithmical accuracy

$$\frac{d\Sigma'_{SC,n}(\omega)}{d\omega}\approx-K\ln\frac{\Delta}{|\omega+2\Delta|}, \tag{35}$$

where $K=\lambda(\mathbf{q}_1)\Delta/[2\omega_{sf}(\mathbf{q}_1)]$. Integrating this formula, we obtain

$$\Sigma'_{SC,n}(\omega)=\Sigma'_{SC,n}(-2\Delta)-K(\omega+2\Delta)\ln\frac{\Delta}{|\omega+2\Delta|}. \tag{36}$$

Note that, contrary to Eq. (23), the singularity in $\Sigma'_{SC,n}(\omega)$ is two-sided, i.e., is symmetric with respect to $\omega+2\Delta$. Substituting this self-energy into the dispersion of a nodal fermion $\omega-\Sigma'(\omega)=v_F(k_\perp-k_F)$, we find that the kink in Σ' gives rise to a kink in the dispersion at $\omega=-2\Delta$, but the *S*-shape form *does not emerge*. We plot $\mathrm{Re}\,\Sigma(\omega)$ and the dispersion in Figs. 5(a) and 5(b).

The inclusion of the momentum dispersion of $\chi_s(\mathbf{q})$ around $\mathbf{q}_1$ affects the prefactor, but the logarithmical singularity near -2Δ survives. Indeed, this singularity is just the consequence of the square-root nonanalyticity in the spin

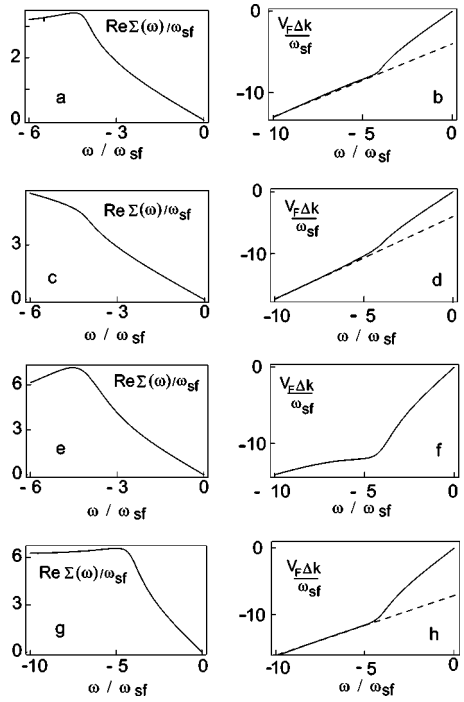

FIG. 5. Re Σ and the dispersion along the nodal direction. (a)–(f) are obtained with $\Pi_{\mathbf{q}}(\omega)$ given by Eq. (14). (a) and (b) are for a flat static spin susceptibility $\chi_s(\mathbf{q})$ near $\mathbf{q}_1$, (c)–(h) for the Ornstein-Zernike form. (c) and (d) are obtained within Eliashberg theory, (e) and (f) assuming a vanishing Fermi velocity at $\mathbf{q}_1$ (anti-Eliashberg approximation). (g) and (h) are obtained using the spin polarization operator, Eq. (47), with an extra threshold at Ω'_{th}. In all cases, the dispersion shows a kink around 2Δ, and does not have the *S*-shape form typical for the antinodal dispersion (see Fig. 4). Dashed lines are extrapolations from high frequencies; the extrapolated dispersion at $\omega=0$ has a negative Δk, i.e., k inside the Fermi surface. The coupling $\lambda(\mathbf{q}_1)=2$ and $\Delta/\omega_{sf}(\mathbf{q}_1)=2$.

polarization operator, which is confined to bosonic frequencies near Δ. At these frequencies; $\Pi_{\mathbf{q}_1}(\omega)$ is small, and the dynamical spin susceptibility can be expanded in powers of $\Pi_{\mathbf{q}_1}(\omega)$. The momentum dependence of $\chi_s(\mathbf{q})$ then just affects the prefactor of the $(\omega+2\Delta)\ln(\omega+2\Delta)$ term in Eq. (36). To verify this, we computed the self-energy and the dispersion for the Ornstein-Zernike form of $\chi_s(\mathbf{q})$. In this situation,

$$\Sigma_{SC,n}(\omega)=\frac{\lambda(\mathbf{q}_1)}{2}\int_{-\infty}^{\infty}d\omega'\frac{\omega'}{\sqrt{(\omega')^2-\Delta^2}}\times\frac{1}{[1-i\sqrt{(\omega+\omega')^2-\Delta^2}/\omega_{sf}(\mathbf{q}_1)]^{1/2}}. \quad (37)$$

Again, at low frequencies

$$\mathrm{Re}\,\Sigma_{SC,n}(\omega)=-\lambda_{sc}(\mathbf{q}_1)\omega, \quad (38)$$

where now $\lambda_{SC}(\mathbf{q}_1)=\lambda(\mathbf{q}_1)\tilde{\psi}(\Delta/\omega_{sf}(\mathbf{q}_1))$, and

$$\tilde{\psi}(x)=\int_0^{\infty}\frac{dz}{(z^2+1)^{3/2}}\frac{1}{(1+x\sqrt{z^2+1})^{1/2}}. \quad (39)$$

Near $\omega=-2\Delta$, we obtain from Eq. (37) the same functional form as in Eq. (36),

$$\Sigma'_{SC,n}(\omega)=\Sigma'_{SC,n}(-2\Delta)-\tilde{K}(\omega+2\Delta)\ln\frac{\Delta}{|\omega+2\Delta|}, \quad (40)$$

where now $\tilde{K}=\lambda(\mathbf{q}_1)\Delta/[4\omega_{sf}(\mathbf{q}_1)]$. We plot the self-energy and the dispersion for the Ornstein-Zernike static susceptibility in Figs. 5(c) and 5(d). We see that the dispersion does not change much from that for a flat $\chi_s(\mathbf{q})$, namely, there is a kink near 2Δ, but there is no *S*-shape dispersion as occurs for an antinodal fermion.

Finally, to verify that the nodal dispersion is not an artifact of our computational procedure, we also computed $\Sigma'_{SC,n}(\omega)$ with the Ornstein-Zernike $\chi_s(\mathbf{q})$ in a different (anti-Eliashberg) computational scheme: we assumed that the Fermi velocity of an antinodal fermion nearly vanishes, and integrated over momenta normal to the Fermi surface in the bosonic rather than the fermionic propagator. In this situation,

$$\Sigma_{SC,n}(\omega)=\frac{-i\Delta\lambda(\mathbf{q}_1)}{2}\int_{-\infty}^{\infty}d\omega'\frac{\omega'}{(\omega')^2-\Delta^2}\times\ln\frac{\omega_{sf}(\mathbf{q}_1)-i\sqrt{(\omega+\omega')^2-\Delta^2}}{\omega_{sf}(\mathbf{q}_1)-i\sqrt{(\omega-\omega')^2-\Delta^2}}. \quad (41)$$

Again, at low frequencies, the self-energy is linear,

$$\mathrm{Re}\,\Sigma_{SC,n}(\omega)=-\lambda_{sc}(\mathbf{q}_1)\omega, \quad (42)$$

where now $\lambda_{SC}=\lambda(\mathbf{q}_1)\psi^*(\Delta/\omega_{sf}(\mathbf{q}_1))$, and $\psi^*(x\ll 1)=x|\ln x|$, and $\psi^*(x\gg 1)=\pi/4$. Near $\omega=\pm 2\Delta$, the derivative $d\Sigma_{SC,n}(\omega)/d\omega$ is again singular, but now

$$\frac{d\Sigma_{SC,n}(\omega)}{d\omega}=-\Delta\lambda(\mathbf{q}_1)\int_{-\infty}^{\infty}d\omega'\frac{\omega'(\omega+\omega')}{[(\omega')^2-\Delta^2+i\delta]}\times\frac{1}{\sqrt{(\omega+\omega')^2-\Delta^2+i\delta}}\times\frac{1}{\omega_{sf}(\mathbf{q}_1)-i\sqrt{(\omega+\omega')^2-\Delta^2}}. \quad (43)$$

Expanding, as before near $\omega=-2\Delta$ and introducing $\omega=-2\Delta+\epsilon$ and $\omega'=\Delta+x$, we obtain from Eq. (43)

$$\frac{d\Sigma_{SC,n}(\omega)}{d\omega}=\frac{\Delta^2\lambda(\mathbf{q}_1)}{2\sqrt{2\Delta}\omega_{sf}(\mathbf{q}_1)}\int_{-\infty}^{\infty}\frac{dx}{x+i\delta}\frac{1}{\sqrt{-\epsilon-x+i\delta}}. \quad (44)$$

Evaluating the integral using Eq. (21) we obtain

$$\frac{d\Sigma_{SC,n}(\omega)}{d\omega}=-\frac{\pi\Delta^2\lambda(\mathbf{q}_1)}{\sqrt{2\Delta}\omega_{sf}(\mathbf{q}_1)}\frac{1}{\sqrt{\omega+2\Delta}}, \quad (45)$$

i.e., near $\omega=-2\Delta$,

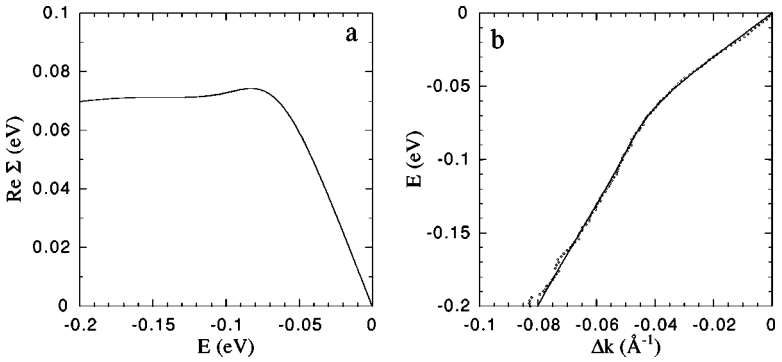

FIG. 6. (a) Re Σ and (b) nodal dispersion generated from the model of Ref. 15. Circles are the experimental data of Ref. 3 for optimal doped Bi2212 at $T=40$ K. The S shape is replaced by a kink due to (1) dominance of the continuum contribution to the self-energy relative to that of the resonance and (2) a strong energy broadening of 40 meV, which was assumed when deriving the self-energy. For these calculations, $\omega_{res}=40$ meV, $\Delta_{(\pi,0)}=40$ meV, and the continuum has a gap of 65 meV and a cutoff of 500 meV. For this direction, the bare Fermi velocity is 3.37 eV Å.

$$\Sigma'_{SC,n}(\omega)=\Sigma'_{SC,n}(-2\Delta)-K^*\ \mathrm{Re}\ \sqrt{2\Delta(\omega+2\Delta)}, \quad (46)$$

where $K^*=\pi\lambda(\mathbf{q}_1)\Delta/[\omega_{sf}(\mathbf{q}_1)]$. As a result, the kink at -2Δ survives, and $\Sigma_{SC,n}(-2\Delta)$ still does not diverge, i.e., there is no S-shape, antinodal-type dispersion. At the same time, the functional form of the nonanalytic piece changes–the $x\ln|x|$ singularity in the real part of the self-energy in Eqs. (36) and (40), where $x=\omega+2\Delta$, gets replaced by a one-sided $\sqrt{x}$ singularity. We plot the self-energy, Eq. (41), and the resulting dispersion in Figs. 5(e) and 5(f). As the two expressions for the self-energy for the Ornstein-Zernike $\chi_s(\mathbf{q})$, Eqs. (37) and (41), represent two extremes of large and small fermionic dispersion compared to the bosonic dispersion, the actual self-energy should be somewhere in between, i.e., it is stronger than that in Eq. (36) for $|\omega|<2\Delta$, and weaker for $|\omega|>2\Delta$. Still, we emphasize that both computational schemes yield a kink in the dispersion, but no divergence of $\mathrm{Re}\,\Sigma(-2\Delta)$ and no S-shape dispersion.

The actual behavior of the dispersion is more involved, as one has to average over all $\mathbf{q}$ for scattering from a node to some other Fermi surface point. This obviously weakens the 2Δ singularity roughly in the same way as the singularity in the density of states at Δ is weakened by the momentum dependence of the gap in a d-wave superconductor. Furthermore, even if by geometrical reasons, node-antinode scattering at $\mathbf{q}_1$ dominates the nodal self-energy, the actual form of $\Sigma_{SC,n}(\omega)$ is more complex than in Eqs. (28), (37), or (41). As we already discussed in Sec. II B 1, the square-root behavior of $\Pi_{\mathbf{q}}(\Omega)$ persists only in a small region near the threshold, while at larger Ω, additional features in $\Pi_{\mathbf{q}_1}(\Omega)$, associated with the existence of two extra pairs of Fermi surface points separated by $\mathbf{q}_1$ become relevant (see Fig. 3).

To qualitatively estimate the relevance of this effect, we model $\Pi_{\mathbf{q}_1}(\Omega)$ in Fig. 3 by a combination of a square-root behavior above $\Omega=\Delta$ and a near discontinuity at $\Omega=1.6\Delta$:

$$\Pi''_{\mathbf{q}_1}(\Omega)\approx\gamma\left[\sqrt{\Omega^2-\Delta^2}+\frac{a}{2}\left(1+\tanh\frac{\Omega^2-(1.6\Delta)^2}{b}\right)\right]. \quad (47)$$

For consistency with Fig. 3, $a\sim 1.2\Delta$, and we set $b\sim 0.1\Delta$ ($b=0$ would correspond to a true discontinuity). In Figs. 5(g) and 5(h), we plot the self-energy and the dispersion for this form of $\Pi_{\mathbf{q}}(\Omega)$ and flat $\chi_s(\mathbf{q})$. We see that the dispersion does not change much compared to that with just a square-root form of $\Pi_{\mathbf{q}_1}(\Omega)$ [see Fig. 5(b)]. There is still a cusp near 2Δ and a non-S-shape dispersion. The only new effect is the extension of the crossover region above the kink. This is indeed expected as the new term in relation (47) affects the polarization operator at higher frequencies.

To summarize this section, we see that the result of various computational procedures is virtually the same: the self-energy of a nodal fermion is much less affected by superconductivity than the self-energy of an antinodal fermion. The nodal self-energy roughly displays the same crossover as in the normal state, from a linear in frequency behavior at small frequencies, to a more flat behavior at higher frequencies. Superconductivity only sharpens the crossover near 2Δ, but does not give rise to any S-shape features in the dispersion.

C. A comparison with Ref. 15

It is instructive to compare our results for nodal fermions with the earlier study by Eschrig and Norman.[15] These authors also argued that the dominant scattering process for a nodal fermion is node-antinode scattering by $\mathbf{q}_1$ [though they included a second process due to node-$(\pi,0)$ scattering]. They used a phenomenological form of the spin susceptibility at $\mathbf{q}_1$ with the resonance piece taken as a Lorenztian of width $2a$ about $\mathbf{q}_0$. The resulting value at $\mathbf{q}_1$ is about 8% of that at $\mathbf{q}_0$. Added to this is a gapped continuum (with a gap equal to the threshold value of $\mathrm{Im}\,\Pi_{\mathbf{q}_0}$) modeled as a step function with an ultraviolet cutoff. This form of $\chi_s(\mathbf{q}_1,\Omega)$ is not exactly the one we used above (in our analysis, the resonance piece is completely absent at $\mathbf{q}_1$), but nevertheless is rather similar in the sense that a large part of the magnetic excitation spectrum is incoherent. Not surprisingly, the two forms for $\chi_s(\mathbf{q}_1,\omega)$ yield similar results for the dispersion of a nodal electron. In Fig. 6, we plot the self-energy and nodal dispersion obtained with their susceptibility. We see that this dispersion has a kink, but no S shape. This was achieved by putting in a significantly large amount of damping that acts to smear out the δ-function singularity in energy of the resonance. An S shape would still be present, though, if the continuum piece is ignored. This result shows that even when the resonance is present, the S shape of the dispersion emerges only when the resonance contribution to $\Sigma'(\omega)$ overshadows the one from the incoherent piece in $\chi_s(\mathbf{q},\Omega)$. This implies, in particular, that the S shape dispersion does

not emerge immediately away from the nodal direction, i.e., it appears somewhere between the nodal and antinodal points.

III. PHONON SCATTERING

We now perform the same analysis for phonon scattering. Consider a system of electrons interacting with an optical phonon with a frequency ω_{ph} and momentum $\mathbf{q}=\mathbf{q}_{ph}$. The optical phonon propagator can be reasonably approximated by

$$\chi_{ph}(\mathbf{q},\omega)=\frac{g(\mathbf{q})}{(\omega+i\gamma)^2-\omega_{ph}^2}, \tag{48}$$

where $g(\mathbf{q})$ rapidly decays at deviations from $\mathbf{q}_{ph}$, and γ is the phonon damping rate. The fermionic self-energy due to electron-phonon scattering is given by Eq. (2), only $3g_s^2$ is replaced by g_{ep}^2. To simplify the discussion, we consider a nodal fermion and assume that the Fermi velocity at $\mathbf{k}_F+\mathbf{q}_{ph}$ can be neglected. Substituting Eq. (48) into the self-energy, we obtain

$$\mathrm{Re}[\Sigma_{nodal}^{ph}(\omega)]=-\frac{\pi\beta\omega}{\omega_{ph}}\frac{(\omega_{th}^2-\omega^2)}{(\omega_{th}^2-\omega^2)^2+4\gamma^2\omega^2}, \tag{49}$$

where $\beta=g_{ep}^2\int g(\mathbf{q})d^2q$ and $\omega_{th}{}^2=(\omega_{ph}+\Delta)^2+\gamma^2$. Solving now for the dispersion, we find that at low energies, the dispersion is linear with $v_F^*=v_F/(1+\lambda_{SC}^{ep})$ and $\lambda_{sc}^{ep}=\pi\beta/(\omega_{ph}\omega_{th}^2)$. Near ω_{th}, the real part of the self-energy for small γ nearly diverges as ω approaches ω_{th}, giving rise to an *S*-shape dispersion.[27] We illustrate this in Fig. 7. The *S* shape could in principle be eliminated if γ is very large, i.e., the bosonic mode is almost overdamped.[28] However, one can easily make sure that to avoid the *S* shape, one requires

$$\frac{\gamma^2}{\omega_{th}^2}>\frac{1}{2}\lambda_{sc}^{ph}. \tag{50}$$

This can be relatively easily achieved at weak coupling, but for $\lambda_{SC}^{ep}\geq 1$, which is required to fit the low-energy renormalizaton, the *S* shape is eliminated only at nonphysical $\gamma\gg\omega_{th}$. Furthermore, for $\lambda_{sc}^{ph}>2$, the *S* shape cannot be eliminated for any γ. If we do not neglect the Fermi velocity at $\mathbf{k}_F+\mathbf{q}_{ph}$, then at the lowest frequencies we obtain qualitatively the same result as Eq. (23), i.e., a nearly one-sided square-root singularity. Again, it is very difficult to get rid of the *S*-shape form of the dispersion at strong coupling without requiring that the bosonic mode is totally overdamped. It is therefore very unlikely that the interaction with an optical phonon can simultaneously account for a strong Fermi velocity renormalization and give rise to a non-*S*-shape form of the dispersion.[29]

IV. CONCLUSIONS AND EXPERIMENTAL COMPARISONS

We conclude therefore that the spin fluctuation scenario more likely explains the observed features in the electron dispersion than the phonon scenario. Within the spin fluctuation scenario: (i) in the normal state, there is a crossover from a linear to a more steep dispersion at around ω_{sf}, (ii) below T_c the antinodal dispersion develops an *S*-shape form due to interaction with the spin resonance with a characteristic energy of $\Delta+\omega_{res}$, (iii) the nodal dispersion below T_c develops a kink at 2Δ, but there is no *S*-shape dispersion as there is no spin resonance for momenta that connect a nodal point with other points on the Fermi surface.

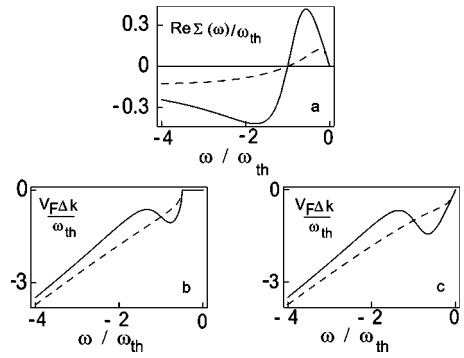

FIG. 7. (a) $\mathrm{Re}\,\Sigma$ and (b) antinodal and (c) nodal dispersion for the electron-phonon interaction. We used Eq. (49) for the self-energy with $\omega_{th}=2\Delta$ and coupling constant $\lambda_{sc}^{ep}=2$. Solid and dashed lines are for $\gamma/\omega_{th}=0.6$ and 2, respectively. For moderate damping, the dispersion along both directions has an *S*-shape form. Note that the extrapolated dispersion crosses the vertical axis at a positive Δk, i.e., for k outside the Fermi surface (Ref. 26). For the spin-fermion interaction, this crossing always occurs at negative Δk for the nodal direction.

A. A comparison with experiments

Qualitatively, our picture of an *S*-shape dispersion in the antinodal region below T_c, and a kink dispersion in the nodal region, which is similar above and below T_c, agrees well with the data.[30] Quantitatively, $\omega_{sf}(\mathbf{q}_0)$ and $\omega_{sf}(\mathbf{q}_1)$ relevant for the antinodal and nodal dispersion, respectively, were estimated to be $\omega_{sf}(\mathbf{q}_0)\sim 20$ meV and $\omega_{sf}(\mathbf{q}_1)\sim 40-50$ meV in Bi2212.[22] Experimentally, this scale has been detected for the nodal dispersion and is around 50 meV. The resonance frequency ω_{res} and the gap Δ in optimally doped Bi2212 are both near 40 meV;[16] hence the termination of the *S* shape in the antinodal dispersion and the kink in the nodal dispersion both occur near 80 meV. Experimentally, this scale is 80 meV along the antinodal direction and $50-70$ meV along the nodal direction.[8] Both of these gap-related scales are smaller in LSCO, but for that material, there are no noticeable differences between the normal and superconducting state dispersions. This implies that the effect of the superconductivity on the dispersion is very small (though it should be noted that most of the "normal state" data for LSCO were actually taken in the pseudogap state, the pseudogap providing a sizable antinodal energy scale[31]). We note in passing that the same smallness was cited as a reason for the nonobservation of the resonance peak in LSCO.[32] Moreover, recent neutron scattering studies[33] find that the spin excitation spectrum in LSCO is remarkably similar to that in YBCO. The universality observed in the spin dynamics and that observed in the photoemission,[4] we would argue, supports a magnetic interpretation of the dispersion anomalies.

B. The doping dependence

Finally, we discuss the doping dependence of the dispersion. There are few systematic studies of the doping dependence along the antinodal direction.[9,10,34] Our study shows that the magnitude of the *S*-shape dispersion should increase with underdoping as $\chi_s(\mathbf{q}_0)$ increases, and the coupling constant gets larger. Along the nodal direction, the low-energy Fermi velocity $v_F^* \sim 1.6$ eV Å is relatively doping independent.[7] In constrast, the slope of the high-energy dispersion monotonically increases with underdoping.[7] Within our theory, the low-energy Fermi velocity is given by $v_F^* = v_F/[1+\lambda(\mathbf{q}_1)]$, and the coupling constant $\lambda(\mathbf{q}_1)$ depends on the spin-fermion coupling g_s and $\chi_s(\mathbf{q}_1)$. The coupling constant is weakly doping dependent. The susceptibility does depend on doping via the magnetic correlation length ξ, but this dependence is nonsingular for the node-antinode $\mathbf{q}_1 \neq \mathbf{q}_0$. Once $|\mathbf{q}_1 - \mathbf{q}_0| > \xi^{-1}$, the doping dependence disappears, and the nodal coupling $\lambda(\mathbf{q}_1)$ saturates at a fixed value. Previous studies by both us and others yielded $\lambda(\mathbf{q}_1) \sim 1$. This yields a bare velocity $v_F \sim 3$ eV Å consistent with band theory.

We believe that the increase of the high-energy slope with underdoping is a separate effect associated with the fact that at high energies, the system progressively develops spin-density wave (SDW) precursors. Indeed, at high energies, the diagonal scattering by the resonance mode at $\mathbf{q}_0$ cannot be neglected. The argument is simple—at high energies, the Green's function of an intermediate fermion can be pulled out from the momentum and frequency integral in Eq. (2), and the fermionic self-energy acquires the same functional form as in the SDW ordered state:

$$\Sigma_{SDW}(\mathbf{k},\omega) \approx \frac{\Delta_{SDW}^2}{\omega - \epsilon_{\mathbf{k}+\mathbf{q}_0}} \tag{51}$$

where $\Delta_{SDW} \propto g_s^2 \int d^2q d\Omega \chi_s(\mathbf{q},\Omega)$ increases with underdoping. This form is valid for $|\omega| \gg \omega_0$. Substituting this self-energy into the dispersion relation, we find after simple algebra that for the negative energies probed in ARPES measurements, the maximum of the MDC dispersion shifts from $\omega \approx \epsilon_{\mathbf{k}}$ to $\omega \approx \epsilon_{\mathbf{k}} - \Delta_{SDW}^2/(\epsilon_{\mathbf{k}+\mathbf{q}_0} - \epsilon_{\mathbf{k}})$. As $\epsilon_{\mathbf{k}} < 0$ and $\epsilon_{\mathbf{k}+\mathbf{q}_0} > 0$, the correction to the velocity is positive, i.e., the diagonal scattering enhances the value of the velocity compared to v_F. As Δ_{SDW} increases, this effect gives rise to a progressively steeper dispersion, in agreement with the data.

A simple way to appreciate the doping dependence of the high-energy dispersion is to realize that the MDC dispersion for a gapped state is almost vertical for $|\omega| < \Delta_{SDW}$, with some weak dispersion due to coherence factors.[11] Thus, as the doping is decreased, and a Mott-Hubbard pseudogap begins to develop, the high-energy dispersion is expected to become increasingly steep.

ACKNOWLEDGMENTS

We acknowledge useful discussions with Girsh Blumberg, Juan Carlos Campuzano, Erica Carlson, Dan Dessau, Hong Ding, Matthias Eschrig, Peter Johnson, Adam Kaminski, and Filip Ronning. A.C. is supported by the NSF-DMR 0240238 and M.N. by the U. S. Dept. of Energy, Office of Science, under Contract No. W-31-109-ENG-38. A.C. is thankful to Argonne National Laboratory for hospitality during the initial stages of this work.

[1] T. Valla, A.V. Fedorov, P.D. Johnson, B.O. Wells, S.L. Hulbert, Q. Li, G.D. Gu, and N. Koshizuka, Science **285**, 2110 (1999).

[2] P.V. Bogdanov, A. Lanzara, S.A. Kellar, X.J. Zhou, E.D. Lu, W.J. Zheng, G. Gu, J.-I. Shimoyama, K. Kishio, H. Ikeda, R. Yoshizaki, Z. Hussain, and Z.X. Shen, Phys. Rev. Lett. **85**, 2581 (2000).

[3] A. Kaminski, M. Randeria, J.C. Campuzano, M.R. Norman, H. Fretwell, J. Mesot, T. Sato, T. Takahashi, and K. Kadowaki, Phys. Rev. Lett. **86**, 1070 (2001).

[4] A. Lanzara, P.V. Bogdanov, X.J. Zhou, S.A. Kellar, D.L. Feng, E.D. Lu, T. Yoshida, H. Eisaki, A. Fujimori, K. Kishio, J.-I. Shimoyama, T. Noda, S. Uchida, Z. Hussain, and Z.-X. Shen, Nature (London) **412**, 510 (2001).

[5] P.D. Johnson, T. Valla, A.V. Fedorov, Z. Yusof, B.O. Wells, Q. Li, A.R. Moodenbaugh, G.D. Gu, N. Koshizuka, C. Kendziora, Sha Jian, and D.G. Hinks, Phys. Rev. Lett. **87**, 177007 (2001).

[6] F. Ronning, T. Sasagawa, Y. Kohsaka, K.M. Shen, A. Damascelli, C. Kim, T. Yoshida, N. P. Armitage, D.H. Lu, D.L. Feng, L.L. Miller, H. Takagi, and Z.-X. Shen, Phys. Rev. B **67**, 165101 (2003).

[7] X. J. Zhou, T. Yoshida, A. Lanzara, P. V. Bogdanov, S.A. Kellar, K.M. Shen, W.L. Yang, F. Ronning, T. Sasagawa, T. Kakeshita, T. Noda, H. Eisaki, S. Uchida, C.T. Lin, F. Zhou, J.W. Xiong, W.X. Ti, Z.X. Zhao, A. Fujimori, Z. Hussain, and Z.-X. Shen, Nature (London) **423**, 398 (2003).

[8] T. Sato, H. Matsui, T. Takahashi, H. Ding, H.-B. Yang, S.-C. Wang, T. Fujii, T. Watanabe, A. Matsuda, T. Terashima, and K. Kadowaki, Phys. Rev. Lett. **91**, 157003 (2003).

[9] T.K. Kim, A.A. Kordyuk, S.V. Borisenko, A. Koitzsch, M. Knupfer, H. Berger, and J. Fink, Phys. Rev. Lett. **91**, 167002 (2003).

[10] A.D. Gromko, A.V. Federov, Y.-D. Chuang, J.D. Koralek, Y. Aiura, Y. Yamaguchi, K. Oka, Y. Ando, and D.S. Dessau, Phys. Rev. B **68**, 174520 (2003).

[11] M.R. Norman, M. Eschrig, A. Kaminski, and J.C. Campuzano, Phys. Rev. B **64**, 184508 (2001).

[12] Ar. Abanov, A.V. Chubukov, and J. Schmalian, Adv. Phys. **52**, 119 (2003).

[13] M.R. Norman and H. Ding, Phys. Rev. B **57**, R11089 (1998).

[14] Ar. Abanov and A.V. Chubukov, Phys. Rev. Lett. **83**, 1652 (1999); Phys. Rev. B **61**, R9241 (2000).

[15] M. Eschrig and M.R. Norman, Phys. Rev. Lett. **85**, 3261 (2000); Phys. Rev. B **67**, 144503 (2003).

[16] M.R. Norman, H. Ding, J.C. Campuzano, T. Takeuchi, M. Randeria, T. Yokoya, T. Takahashi, T. Mochiku, and K. Kadowaki, Phys. Rev. Lett. **79**, 3506 (1997).

[17] H.F. Fong, P. Bourges, Y. Sidis, L.P. Regnault, J. Bossy, A. Ivanov, D.L. Milius, I.A. Aksay, and B. Keimer, Phys. Rev. B **61**, 14773 (2000); Pengcheng Dai, H.A. Mook, R.D. Hunt, and F. Doğan, *ibid.* **63**, 054525 (2001).

[18] R.J. McQueeney, Y. Petrov, T. Egami, M. Yethiraj, G. Shirane, and Y. Endoh, Phys. Rev. Lett. **82**, 628 (1999).

[19] Ar. Abanov, A.V. Chubukov, and J. Schmalian, J. Electron Spectrosc. Relat. Phenom. **117**, 129 (2001); A.V. Chubukov, D. Pines, and J. Schmalian, in *The Physics of Superconductors*, edited by K.H. Bennemann and J.B. Ketterson (Springer, Berlin, 2003), Vol. 1, p. 495.

[20] See, e.g., A.J. Millis, H. Monien, and D. Pines, Phys. Rev. B **42**, 167 (1990).

[21] The ω^2 regime for $\mathrm{Im}\,\Sigma$ is rather narrow in energy and will be washed out by finite temperature effects, precluding their observation experimentally except in the heavily overdoped limit.

[22] R. Haslinger, Ar. Abanov, and A. Chubukov, Europhys. Lett. **58**, 271 (2002).

[23] M.R. Norman, Phys. Rev. B **61**, 14751 (2000) and references therein.

[24] P. Bourges, Y. Sidis, H.F. Fong, L.P. Regnault, J. Bossy, A. Ivanov, and B. Keimer, Science **288**, 1234 (2000).

[25] See e.g., J.P. Carbotte, Rev. Mod. Phys. **62**, 1027 (1990).

[26] A similar observation has been made by B. Farid, Philos. Mag. **84**, 909 (2004).

[27] This *S* shape from phonons is obvious in earlier work as well; see S. Verga, A. Knigavko, and F. Marsiglio, Phys. Rev. B **67**, 054503 (2003); E. Schachinger, J. J. Tu, and J. P. Carbotte, *ibid.* **67**, 214508 (2003); A.W. Sandvik, D.J. Scalapino, and N.E. Bickers, *ibid.* **69**, 094523 (2004).

[28] In real materials, the phonon density of states has a large spread in energy which also acts to smear the *S* shape; see Verga *et al*. and Schachinger *et al*. of Ref. 27. However, this broadening also reduces the renormalization of the Fermi velocity, as can be seen from Eq. (49).

[29] But if the bare Green's function is assumed to be a Luttinger liquid, then the *S* shape from an Einstein mode is also smeared out; see I.P. Bindloss and S.A. Kivelson, cond-mat/0402457 (unpublished).

[30] Similar results have been obtained from FLEX calculations by D. Manske, I. Eremin, and K.H. Bennemann, Phys. Rev. Lett. **87**, 177005 (2001); Phys. Rev. B **67**, 134520 (2003).

[31] X.J. Zhou, T. Yoshida, D.-H. Lee, W.L. Yang, V. Brouet, F. Zhou, W.X. Ti, J.W. Xiong, Z.X. Zhao, T. Sasagawa, T. Kakeshita, H. Eisaki, S. Uchida, A. Fujimori, Z. Hussain, and Z.-X. Shen, Phys. Rev. Lett. **92**, 187001 (2004).

[32] E. Demler, S. Sachdev, and Y. Zhang, Phys. Rev. Lett. **87**, 067202 (2001).

[33] J.M. Tranquada, H. Woo, T.G. Perring, H. Goka, G.D. Gu, G. Xu, M. Fujita, and K. Yamada, Nature (London) **429**, 534 (2004); N.B. Christensen, D.F. McMorrow, H.M. Ronnow, B. Lake, S.M. Hayden, G. Aeppli, T.G. Perring, M. Mangkorntong, M. Nohara, and H. Tagaki, Phys. Rev. Lett. **93**, 147002 (2004).

[34] J.C. Campuzano, H. Ding, M.R. Norman, H.M. Fretwell, M. Randeria, A. Kaminski, J. Mesot, T. Takeuchi, T. Sato, T. Yokoya, T. Takahashi, T. Mochiku, K. Kadowaki, P. Guptasarma, D.G. Hinks, Z. Konstantinovic, Z.Z. Li, and H. Raffy, Phys. Rev. Lett. **83**, 3709 (1999).